Light Metals 2015
Edited by: Margaret Hyland
TMS (The Minerals, Metals & Materials Society), 2015

MACROSEGREGATION DURING DIRECT CHILL CASTING OF ALUMINUM ALLOY 7050

Kyle Fezi, John Coleman, Matthew J. M. Krane
Purdue Center for Metal Casting Research, School of Materials Engineering, Neil Armstrong Hall of Engineering,
701 Northwestern Avenue, Purdue University, West Lafayette, IN 47907, USA

Keywords: Direct Chill Casting, Macrosegregation, Alloy 7050

Abstract

A fully transient numerical model of the direct chill casting process is used to examine the influence of casting parameters on the macrosegregation of alloy 7050. The casting speed and secondary cooling boundary condition were varied. The secondary cooling was altered by placing a wiper to divert the free-falling water away from the solidified metal surface. Both the casting rate and wiper placement affect the sump depth and shape, and therefore influence the level of macrosegregation, especially at the centerline. The sump depth and level of macrosegregation increased with the casting rate, while placing the wiper nearer the mold could decrease negative centerline segregation.

Introduction

The most common processing method for wrought aluminum alloys is direct chill (DC) casting. The severe heat transfer that occurs during DC casting causes large thermal stresses and strains which can crack the ingot. One way to mitigate thermal stresses is implementation of a wiper to divert the free falling water. Wipers have been shown to affect the sump depth and reduce measured internal stresses by 33% [1,2]. However, the effect of using a wiper on liquid metal flow and macrosegregation has not been investigated. In this study, a continuum mixture model for the conservation of mass, energy, species, and momentum is used. The model is coupled with a multicomponent solidification model to simulate the production of alloy 7050 billets. Different casting speeds are investigated with various wiper placements to gain insight into the mechanisms that contribute to macrosegregation.

Numerical Model

Model Description

The momentum equations for the fluid flow in DC casting are taken from the model of Vreeman et al. [3], who included the effect of free-floating solid grains forming when the local temperature is below the liquidus temperature. These equations are for the mixture velocities, which are a solid mass fraction weighted average of the solid and liquid velocities. The mass and momentum equations in axisymmetric coordinates are:

$$\frac{\partial}{\partial t}(\rho)+\nabla\bullet\left(\rho\vec{V}\right)=0 \tag{1}$$

$$\begin{aligned}&\frac{\partial}{\partial t}(\rho u)+\nabla\bullet\left(\rho\vec{V}u\right)=\nabla\bullet\left(\mu_l\frac{\rho}{\rho_l}\nabla u\right)+\nabla\bullet\left(\mu_l u\nabla\left(\frac{\rho}{\rho_l}\right)\right)\\&-\nabla\bullet\left(\mu_l\frac{\rho f_s}{\rho_l}\nabla u_s\right)-\nabla\bullet\left(\mu_l u_s\nabla\left(\frac{\rho f_s}{\rho_l}\right)\right)+\nabla\bullet\left(\mu_l u_s\nabla g_s\right)\\&+\nabla\bullet\left(\mu_s g_s\nabla u_s\right)-\nabla\bullet\left[\left(\frac{\rho f_s}{f_l}\right)\left(\vec{V}-\vec{V}_s\right)\left(u-u_s\right)\right]+\rho\mathrm{B}_z-\frac{\partial P}{\partial z}\end{aligned} \tag{2}$$

$$\begin{aligned}&\frac{\partial}{\partial t}(\rho v)+\nabla\bullet\left(\rho\vec{V}v\right)=\nabla\bullet\left(\mu_l\frac{\rho}{\rho_l}\nabla v\right)-\mu_l\frac{\rho}{\rho_l}\frac{v}{r^2}\\&+\nabla\bullet\left(\mu_l v\nabla\left(\frac{\rho}{\rho_l}\right)\right)-\nabla\bullet\left(\mu_l\frac{\rho f_s}{\rho_l}\nabla v\right)+\mu_l\frac{\rho f_s}{\rho_l}\frac{v}{r^2}\\&-\nabla\bullet\left(\mu_l v\nabla\left(\frac{\rho f_s}{\rho_l}\right)\right)+\nabla\bullet\left(\mu_l v\nabla g_s\right)+\nabla\bullet\left(\overline{\mu}_s g_s\nabla v\right)\\&-\overline{\mu}_s g_s\frac{v}{r^2}-\frac{\partial P}{\partial r}\end{aligned} \tag{3}$$

The conservation equations are solved on a staggered grid using the finite volume method and the SIMPLER algorithm for the flow field [4]. Solid is assumed to form initially as free-floating equiaxed particles, but once a critical fraction solid, $g_{s,crit}$, is reached the free floating solid particles coalesce to form a rigid, permeable solid structure at which point u_s=v_s=0 in equations (1)-(3). The critical fraction solid (or packing fraction), is generally a difficult to determine quantity related to the size and morphology of the equiaxed dendrites and the direction and strength of the liquid flow [5]. The packing fraction has been observed to be below 30% [6,7] and for this study a value of 15% is used.

The flow is driven primarily by thermal and solutal buoyancy effects and by density differences between the solid and liquid, as seen in ρB_z term in the axial momentum equation (2):

$$\begin{aligned}\rho\mathrm{B}_z&=g_s\left(\rho_s-\rho_l\right)g\\&-g_s\rho_s g\left[\beta_{T,s}\left(T-T_0\right)+\beta_{S,s}\left(C_s^i-C_0^i\right)\right].\\&-g_l\rho_l g\left[\beta_{T,l}\left(T-T_0\right)+\beta_{S,l}\left(C_l^i-C_0^i\right)\right]\end{aligned} \tag{4}$$

Only the last term is used when the solid is packed ($g_S > g_{S,crit}$).

The fluid is also impelled by the step change of density when liquid forms solid and this shrinkage induced flow is modeled by changes in the mixture density (ρ) in the continuity equation (1). The relative velocity of the solid and liquid is related by Stokes law:

$$\vec{V}_s-\vec{V}_l=\frac{\left(1-g_s\right)}{18\mu_m}\left(\rho_s-\rho_l\right)d^2\vec{g}\,, \tag{5}$$

in which d is the average particle diameter and μ_m is the mixture viscosity. This equation treats the equiaxed dendrites as uniform solid spheres of a specified diameter.

While the free-floating solid does not impede the fluid motion, the packed, rigid solid dendrites slow the flow in the metal mushy zone. The Blake-Kozeny model is used here to model flow through the mushy zone, where the permeability (K) is a function of the secondary arm spacing (λ_2) and the volume fraction solid (g_s):

$$K = \frac{\lambda_2^2}{180}\frac{(1-g_s)^3}{g_s^2}. \tag{6}$$

When the mushy zone is rigid ($g_s > g_{s,crit}$), the terms $\frac{\mu\rho}{K\rho_l}u$ and $\frac{\mu\rho}{K\rho_s}v$ are added to equations (2) and (3), respectively, to represent the drag due to the packed dendrites.

The species and energy conservation equations are given by:

$$\begin{aligned}&\frac{\partial}{\partial t}\left(\rho C^i\right)+\nabla\bullet\left(\rho f_l\vec{V}C^i\right)=\nabla\bullet\left(\rho f_l D\nabla C^i\right)\\&+\nabla\bullet\left(\rho D\nabla\left(C_l^i-C^i\right)\right)-\nabla\bullet\left(\rho f_s\vec{V}\left(C_l^i-C^i\right)\right)\end{aligned} \tag{7}$$

and

$$\begin{aligned}&\frac{\partial}{\partial t}\left(\rho c_p T\right)+\nabla\bullet\left(\rho c_p T\vec{V}\right)=\nabla\bullet\left(k\nabla T\right)-\frac{\partial}{\partial t}\left(\rho f_l L_f\right)\\&-\nabla\bullet\left(\rho f_l L_f\vec{V}\right)-\nabla\bullet\left(\rho f_s\left(\left(c_{pl}-c_{ps}\right)T+L_f\right)\left(\vec{V}-V_s\right)\right)\end{aligned}. \tag{8}$$

Aluminum alloy 7050 was assumed to have a nominal composition of Al – 6.2Zn – 2.3Cu – 2.25Mg – 0.12Zr – 0.075Fe – 0.06Si – 0.03Ti – 0.02Cr – 0.05Mn (in wt. %), based on ASTM B247. Only four of these elements are modeled in this work (Al, Zn, Cu, Mg), chosen based on their contributions to solutal buoyancy and segregation characteristics. The function for the liquidus temperature used in the thermodynamic model was:

$$T = 933.15+0.63-174.16C_l^{Zn}-271.55C_l^{Cu}-494.68C_l^{Mg} \tag{9}$$

The first two terms in equation (9) are the melting temperature of pure Al and an adjustment to the liquidus temperature due to the trace elements not tracked in the model (Zr, Fe, Si, Ti, Cr, and Mn) and assumed to be constant. The partition coefficients ($k = C_s/C_l$) for the alloying elements were found to be

$$k^{Zn}=0.39,\ k^{Cu}=0.09,\text{ and }k^{Mg}=0.29. \tag{10}$$

The temperature function (9) and the partition coefficients (10) are calculated by the thermodynamic database program Thermo-Calc^{TM} using the TCAL1 database.

For simplicity, the metal is assumed to follow lever-rule solidification. Since Scheil and lever-rule only deviate at high fraction solids where the flow in the mushy zone is weak, the effect on the macrosegregation is minor [8]. Depending on the mixture composition of the metal in a given control volume, the metal undergoes primary solidification, or primary solidification followed by an isothermal eutectic reaction. The isothermal reaction occurs when the mixture composition depresses the solidus below the eutectic temperature, 755 K, either by solute transport or by setting the initial compositions in the eutectic reaction regime. Other relevant thermophysical properties are shown in Table 1.

Table 1: Thermophysical properties of aluminum alloy 7050.

Liquid Density [kg/m3]	[9]	2515.0
Solid Density [kg/m3]	[9]	2744.1
Specific Heat [J/kg K]	[9]	1141.0
Latent Heat [J/kg]	[9]	$3.76\text{x}10^5$
Liquid Thermal Conductivity [W/mK]	[9]	83.2
Solid Thermal Conductivity [W/mK]	[9]	149.4
Liquid Viscosity [kg/m s]	[10]	0.0013
Average Solid Viscosity [kg/m s]	[11]	$4.53\mu_l$
Liquid Thermal Expansion [1/K]	[12]	$1.5\text{x}10^{-4}$
Solid Thermal Expansion [1/K]	[9]	$2.29\text{x}10^{-5}$
Liquid Solutal Expansion [1/K]	[12]	Zn: -0.65 Cu: -0.75 Mg: 0.53
Solid Solutal Expansion [1/K]	[10]	Zn: -1.43 Cu: -2.01 Mg: 0.31

Boundary and Initial Conditions

The simulation domain extends from the bottom block (just outside the domain) to the top of the mold. Molten metal is added to the top of the domain to feed the casting speed and solidification shrinkage. The coordinate system is fixed to the bottom of the ingot, and so the frame of reference moves with the ingot. In order to accommodate the expanding domain due to addition of molten metal, a volume of fluid (VOF) method is used to allow for a smooth transition when an additional row of control volumes is added to the domain. This VOF method tracks an artificial interface between two fluids, metal and air at the top of the domain and its details are explained by Yanke et al. [13].

Initially the metal level fills the mold, consisting of a hot top, a graphite ring, and an aluminum mold, shown schematically in Figure 1, along with the dimensions and various thermal boundary conditions. The heat transfer coefficients along the mold wall are functions of the fraction solid of the control volume next to the surface. This adjustment allows for the effect of solidification shrinkage pulling the metal away from the mold. Below the mold, the ingot is actively cooled by water jets and free falling water. The boundary conditions for the water jets are taken from Weckman and Niessan [14]. Below the wiper the heat transfer is assumed to be driven only by natural convection in air, with a heat transfer coefficient of 5 W/mK. The entire domain is set to the superheated pouring temperature of 950 K (677°C) and the initial composition. To develop a solid shell near the mold wall before moving the bottom block, the liquid metal is initially held in the mold for one minute. The casting speed is then set to 50% of the steady state value and linearly increased to steady state so that when reached, the axial length has grown by the radius of the ingot.

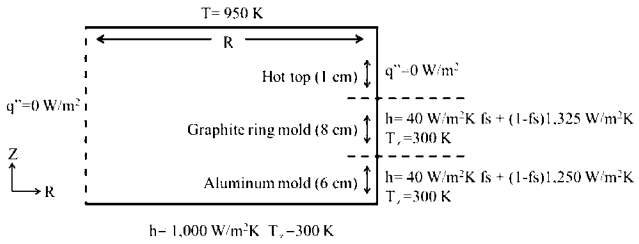

Figure 1: Schematic of the simulation domain showing dimensions and thermal boundary conditions of the mold.

Results and Discussion

The DC casting model has been used to study the startup and steady state regions of alloy 7050 ingots under three different casting speeds using a variety of wiper positions. The results presented here give insight into the effect of wiper position on the macrosegregation and thermal behavior of the developing ingot. The standard operating conditions for this study are shown in Table 2.

Table 2: Standard operating parameters for DC casting simulations of 7050 rounds.

Casting Velocity	V_c	60 mm/min
Ingot Diameter	D	0.7 m
Wiper Position Below Mold	L_w	0.52 m
Jet Water Flow Rate	$\dot{m}$	0.00416 m^3/s

The purpose of the wiper is to divert the falling water from the metal surface, thereby slowing the heat extraction from the ingot and hopefully reducing the transient thermal stresses in the mushy zone and the solid metal. The current model is not capable of predicting the effect of the wiper on the stress fields, so only its influence on the temperature and composition fields will be discussed here.

The standard conditions were simulated with the wiper placed 0.17 m, 0.52 m, and 0.86 m below the mold and one simulation was run with no wiper. The segregation, temperature, and flow fields and the solidification fronts are seen in Figure 2. The case without a wiper (Figure 2a) shows a typical DC casting result, with a sump depth (from inlet to packed solid mushy zone at the centerline) just over 0.5 m and a solidus depth at the centerline just under 1 m. The buoyancy driven flow in the sump penetrates to near the centerline and causes an increase in composition at midradius. Most of the strength of this sump flow is generated by the very strong rate of heat extraction in the mold; the secondary cooling has only a secondary effect on that velocity. Shrinkage induced flow deep in the mush at the centerline and the deposition of solid grains there swept from the outer radius both contribute to a negative centerline segregation in the solid ingot [6]. A radial segregation profile is shown in Figure 3.

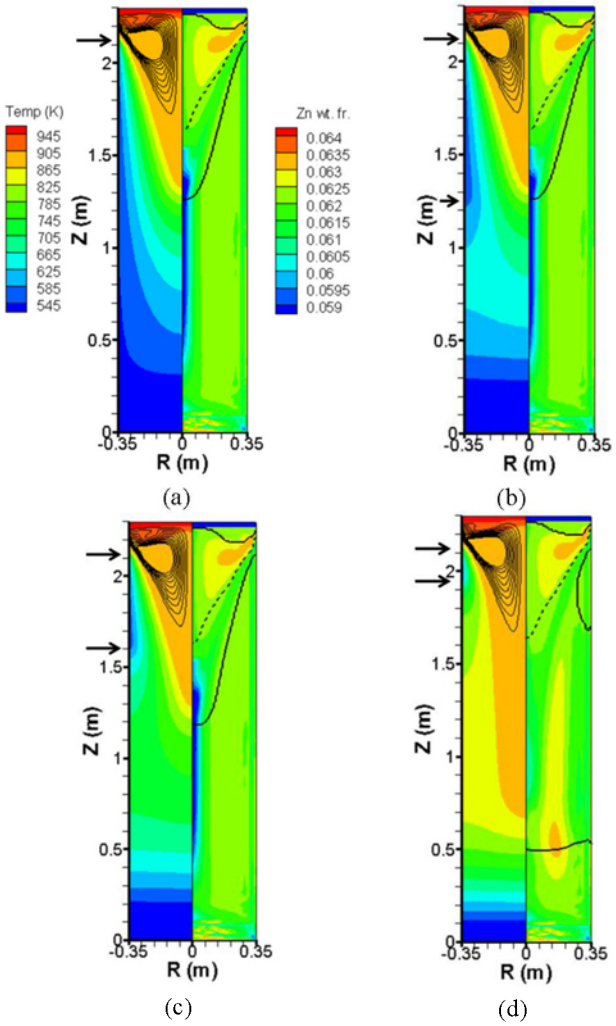

Figure 2: The effect of wiper position on temperature and Zn fields for V_c = 60 mm/min: (a) no wiper, (b) L_w = 0.86m, (c) L_w = 0.52m, and (d) L_w = 0.17m. Top arrows show the bottom of the mold and the bottom arrows the wiper location. In each plot, the Zn composition and sump are on the right, solid lines represent the liquidus and solidus, and the dotted line the packing location of the free-floating solid. On the left are liquid flow streamlines, in which $0.1 < \rho\Psi < 1$ and $\Delta\rho\Psi$=0.1 kg/s, and temperature.

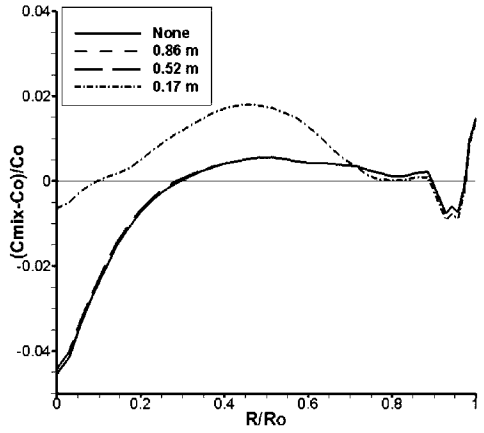

Figure 3: Normalized radial profile of the Zn segregation 0.485 m from the bottom block for V_c = 60 mm/min, comparing the effect of the distance of the wiper from the mold.

In Figure 2b, we can see the effect of adding the wiper at 0.86 m below the mold, which is approximately at the bottom of the packed region at the centerline. The sump remains unaffected by this positioning of the wiper, however the temperature field in the solid region shows some effects. The outer region of the ingot is cold enough to absorb enough heat so the temperature at the centerline behaves as if there was no wiper. However, the lack of significant heat removal below the wiper eventually heats up the outer regions, causing a rise in temperature at the surface (see around z = 0.9 m in Figure 2b).

When the wiper was placed 0.52 m below the mold (Figure 2c), the shape of the slurry region (the dashed line) and solidus are unchanged, as the first is dominated by the strong downward flow in the sump and the second by heat still moving from the center to the outer region. However, the surface temperature rebound is much higher (almost 100°C) and occurs above the last liquid to freeze in this case. Moving the wiper very close to the mold (L_w = 0.17 m) allows very little time to extract heat using the falling secondary cooling water (Figure 2d). In this case, the outer volume is not cold enough to absorb the center's heat without a significant rebound in surface temperature (200 °C). That rebound, coupled with the fact that the surface temperature only dropped to around 350°C at its coldest, means that a large region below the slurry-filled sump never completely freezes until affected by the cold starting block below. In fact, the solid shell at the surface in this case begins to remelt, making the billet susceptible to bleed outs or, at the least, increasing the possibility of an enlarged liquation layer and associated surface defects. On the positive side, because the solidus surface and most isotherms deep in the mushy zone are mostly horizontal, the shrinkage induced centerline segregation is almost entirely eliminated (although the midradius segregation is slightly higher in this case). This last wiper position is the only one of the three simulated that had any noticeable effect on the segregation profile. Based on the current set of results, placing the wiper 0.52 m from the bottom of the mold has the greatest effect on reducing thermal gradients (and thereby reducing thermal stresses) without remelting the aluminum shell.

Similar variations of wiper position were simulated for slower and faster casting velocities. The results for V_c = 30mm/min with L_w = 0.52 m, 0.17 m, and 0.08 m are shown in Figures 4 and 5. Due to the slower casting rate, the sump depth is shallower than in Figure 2 and so the wiper positioned 0.52 m below the mold is well below the bottom of the sump (Figure 4a). As at the higher V_c, putting the wiper near the bottom of the sump has little effect on the sump shape, or the temperature distribution, and there is some small rebound in the outer regions of the ingot. Figure 4b shows results for L_w = 0.17 m. Positioning the wiper closer to the mold (and higher in the sump) causes the solidus line to become steeper and the penetrate deeper in the ingot. The temperature rebound is still moderate and the temperature gradients are much reduced. However, if the wiper is positioned too close to the mold (Figure 4c), the aluminum shell begins to remelt, which again could lead to bleed outs or renewed formation of an exudation layer. The depth of the liquid sump is the same in all three cases. Figure 5 shows the radial segregation profile at a height of 0.695 m for all three cases at 30 mm/min. The results here are similar to the faster casting rate. Out of the three wiper positions examined, positioning the wiper 0.17 m below the mold appears to have the largest effect on lowering temperature gradients without causing the shell to remelt, and even has a small lessening of the centerline segregation. A complete simulation of the stresses under these conditions will be needed to evaluate the effect of these thermal changes due to the wiper and is underway.

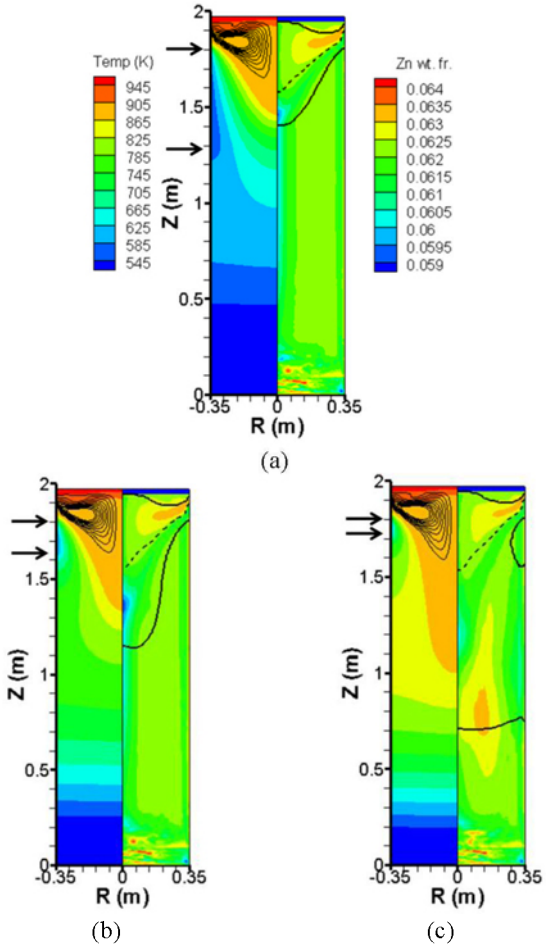

Figure 4: The effect of wiper position on temperature and Zn fields for V_c = 30 mm/min and wiper positions of (a) L_w = 0.52m, (b) L_w = 0.17m, and (c) L_w = 0.08m. The top arrows show the bottom of the mold and the bottom arrows the wiper location.

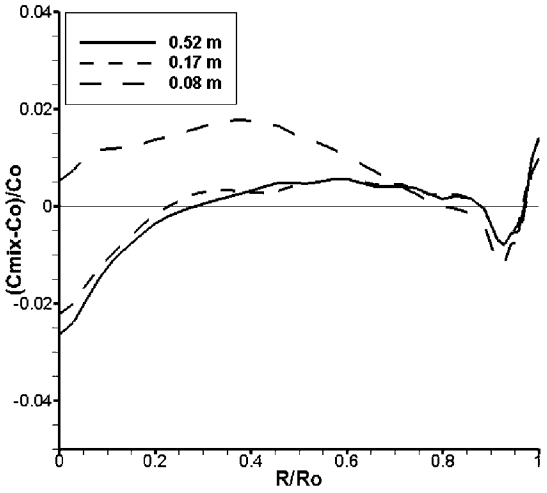

Figure 5: Normalized radial profile of the Zn segregation 0.695 m from the bottom block for V_c = 30 mm/min, comparing the effect of the distance of the wiper from the mold.

Increasing the casting speed to 90 mm/min significantly deepens the sump depth and the position of the solidus at the centerline. Placing the wiper at L_w = 0.17 m (Figure 6b) causes the aluminum shell to remelt. Moving the wiper to L_w = 0.52 m allowed the solid shell to remain intact, but the depth of the solidus line is about two diameters deep. Having such a deep mushy zone causes the billet to be susceptible to a larger degree of macrosegregation due to centerline shrinkage. For this casting speed, as with the slower ones, positioning the wiper in the lower half of the sump seems to be the best choice.

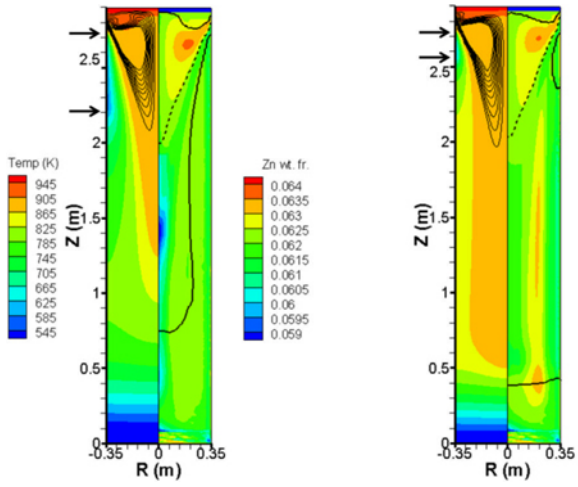

(a) (b)

Figure 6: The effect of wiper position on temperature and Zn fields for V_c = 90mm/min and (a) L_w = 0.52m and (b) L_w = 0.17m. The top arrows show the bottom of the mold and the bottom arrows the wiper location.

Summary

A fully transient numerical model for DC casting has been developed to examine the influence of a wiper for various casting speeds on the fluid flow and macrosegregation. The wiper had very little effect on the liquid sump shape or flow field. When the wiper was placed below the bottom of the sump, there was no effect on segregation or solidification pattern in the rigid mushy zone. There was a small decrease in the temperature gradients near the solid surface. When the wiper was placed in the upper half of the liquid sump, the surface temperature rebounds enough to partially remelt the solid surface. This opens the door for worsened liquation-related surface defects and possible bleed-outs. When the wiper was placed in the lower half of the sump, the surface temperature gradients are much lower and no remelting of the solid occurs.

Acknowledgements

Financial support for this research from Shandong Nanshan Aluminum Co., Beijing Nanshan Institute of Aeronautical Materials, is gratefully acknowledged.

References

[1] J. Drezet, P. Celle, O. Ribaud, and T. Pirling: in *Light Metals*, J. Grandfield, ed., TMS, 2014, pp. 893–98.
[2] Y. Xu, J.C. Wang, S.J. Guo, X.T. Li, and G.X. Xue: *J. Mater. Proc. Tech.*, 2011, vol. 211, pp. 78–83.
[3] C.J. Vreeman, M.J.M. Krane, and F.P. Incropera: *Int. J. Heat Mass Transf.*, 2000, vol. 43, pp. 687–704.
[4] S.V. Patankar: *Numerical Heat Transfer and Fluid Flow*, Hemisphere Publishing, Washington DC, 1980.
[5] I. Vusanovic and M.J.M. Krane: *3rd Int. Conf. Adv. Solidif. Process.*, 2011, vol. 27, 012069.
[6] C.J. Vreeman and F.P. Incropera: *Int. J. Heat Mass Transf.*, 2000, vol. 43, pp. 687–704.
[7] C.J. Vreeman, J.D. Schloz, and M.J.M. Krane: *J. Heat Transfer*, 2002, vol. 124, p. 947.
[8] M.C. Schneider and C. Beckermann: *Int. J. Heat Mass Transf.*, 1995, vol. 38, pp. 3455–73.
[9] M. Lalpoor, D.G. Eskin, D. Ruvalcaba, H.G. Fjær, A. Ten Cate, N. Ontijt, and L. Katgerman: *Mater. Sci. Eng. A*, 2011, vol. 528, pp. 2831–42.
[10] W.F. Gale: *Smithells Metals Reference Book*, 8th ed., Elsevier, 2004.
[11] C.J. Vreeman: M.S. Thesis, Purdue University, 1997.
[12] T Iida and R Guthrie: *The Physical Properties of Liquid Metals*, Clarendon Press, Oxford, 1988.
[13] J. Yanke, K. Fezi, R.W. Trice, and M.J.M. Krane: *Numer. Heat Transf. A.*, 2014, in press.
[14] D.C. Weckman and P. Niessan: *Metall. Mater. Trans. B*, 1982, vol. 13, pp. 593–602.